Progress In Electromagnetics Research Letters, Vol. 71, 133–140, 2017

Design of Dual-Band Bandstop Filter Based on Dumbbell-Shaped Resonators and U-Shaped Slot

Xueliang Min* **and Hou Zhang**

Abstract—A novel dual-band bandstop filter based on a square, symmetric dumbbell-shaped resonator and U-shaped slot defected ground structure is presented. First, the characteristic of the fundamental structure which adopts two dumbbell-shaped resonators and one U-shaped slot is analyzed. Simulated results demonstrate that the proposed structure induces two transmission zeros within 2–8 GHz. Then, the structure adopting four dumbbell-shaped resonators and one U-shaped slot is analyzed. Simulated results point out that the characteristic of dual stopbands is better than the fundamental structure. Based on above implementation, a dual-band bandstop filter based on eight proposed dumbbell-shaped resonators and two U-shaped slots is proposed and fabricated. Two center frequencies at 4 and 6.5 GHz are reported, corresponding to the attenuation levels of 41.9 and 26.1 dB. The return losses of center frequencies are 0.04 and 0.20 dB, respectively, and the dual stopband bandwidths with 10 dB signal attenuation are 690 MHz and 250 MHz. In addition, two transmission poles at each stopband are induced for better selectivity. Owing to the symmetric dumbbell shape, the size of the filter gets reduced. It is simple to design and quite compatible with planar construction fabrication.

1. INTRODUCTION

Owing to the development of microwave communication systems, multi-band bandstop filters are attractive for their performance in preventing several unwanted signals. In recent years, many dual-bandstop filters have been proposed [1–8]. The designs using resonators [9–13] have received increasing interest in recent years. They are implemented on the top layer of the substrate. Near the resonance frequency, the resonators can be modeled by a parallel capacitor and inductor. Defected ground structures have the characteristic of bandstop, and they can also be modeled by a parallel capacitor and inductor. In addition, defected ground structure is usually compact in size. Owing to these advantages, various filters adopting different defected ground structures have been realized [14–19].

In this letter, dumbbell-shaped resonators and U-shaped defected ground structure are integrated in one structure to realize dual-band bandstop filter. First, based on the parametric analysis, the characteristics of the structure adopting two resonators and one U-shaped slot are analyzed. Then, the structure adopting four resonators gets analyzed. Based on above implementation, the dual-band bandstop filter adopting eight dumbbell-shaped resonators and two U-shaped slots is machined. The characteristics of stopband are controlled by adjusting the size of resonators and coupling between the resonators and the U-shaped slot.

The paper is organized as follows. In Section 2, the characteristics of the dumbbell-shaped resonators and U-shaped defected ground structure are analyzed. In Section 3, the proposed filter is presented and fabricated. The equivalent circuit model is developed. In addition, the surface current distribution and measured results are demonstrated.

Received 18 September 2017, Accepted 31 October 2017, Scheduled 21 November 2017
* Corresponding author: Xueliang Min (MinXL08@163.com).
The authors are with the Missile Institute of Airforce Engineering University, Xi'an, Shaanxi Province 710051, China.

2. CHARACTERIZATION OF DUMBBELL-SHAPED RESONATOR AND U-SHAPED DGS

The configuration of the dumbbell-shaped resonator is shown in Figure 1. Compared with the unfolded structure, it is compact. In Table 1, the dimensions of the structure are plotted. Through using proposed resonator coupled to the main microstrip line, stopband can be realized. The dumbbell-shaped resonator can be modeled as a parallel LC resonance circuit. The equivalent capacitance C_0 and inductance L_0 can be expressed as [16]

$$C_0 = \frac{1}{2\pi Z_0(f_u - f_l)} \tag{1}$$

$$L_0 = \frac{1}{4\pi^2 f_0^2 C_0} \tag{2}$$

where f_l and f_u are lower and upper cutoff frequencies at 10 dB, and Z_0 is the characteristic impedance of the transmission line. The effective inductance and capacitance of the equivalent LC circuit model can be approximately calculated by $L_0 = 22.37$ pH, $C_0 = 24.49$ pF. To demonstrate the validity of the proposed parallel LC resonance circuit and the calculated results of L_0 and C_0, the simulated S-parameters from the equivalent circuit and full-wave simulation are compared, as shown in Figure 2. According to the comparison results, the provided circuit and calculated results are applicative to the dumbbell-shaped resonator.

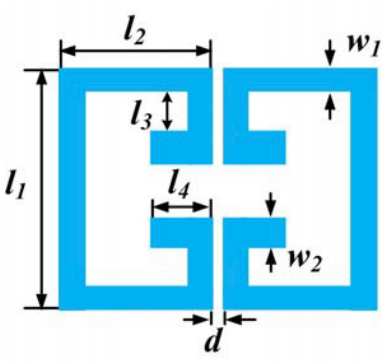

Figure 1. Configuration of symmetric dumbbell-shaped resonator.

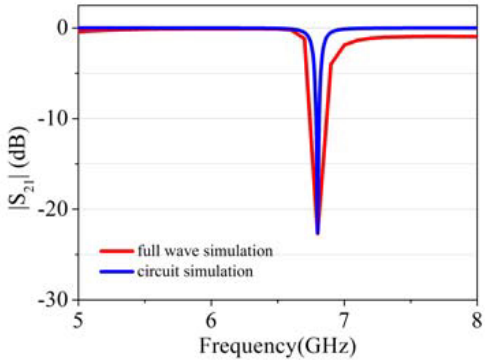

Figure 2. Comparison results of the simulated S-parameters of the equivalent circuit and full-wave simulation.

Table 1. Dimensions of the dumbbell-shaped resonator (Units: mm).

Dimension	Size (mm)	Dimension	Size (mm)
l_1	4.6	w_1	0.5
l_2	2.9	w_2	0.6
l_3	0.7	d	0.1
l_4	1.2		

The U-shaped defected ground structure can also be modeled as parallel LC resonance circuits in accordance with other defected ground structures [17–19]. The equivalent LC circuit model with parameters L_1, C_1 is determined from the cutoff frequency w_c, resonance frequency w_0 and magnitude of S_{21} at resonance. In this case, C_1 is equal to 4.08 pF and L_1 equal to 0.39 nH.

The configuration of the fundamental structure adopting two dumbbell-shaped resonators and one U-shaped DGS is shown in Figure 3. The transmission line and dumbbell-shaped stepped-impedance

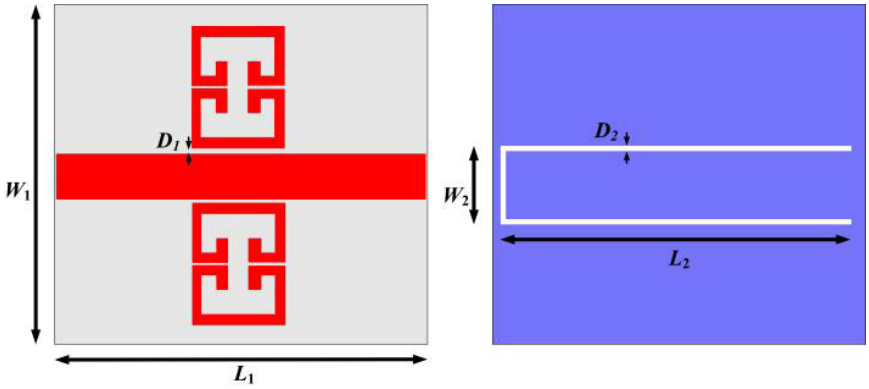

Figure 3. Configuration of the structure adopting two dumbbell-shaped resonators and one U-shaped DGS. (a) Top view. (b) Bottom view.

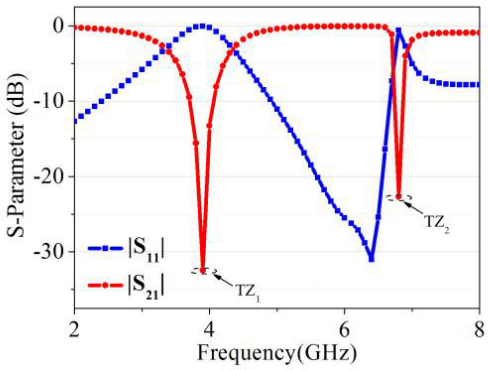

Figure 4. The S-parameter curves of the structure.

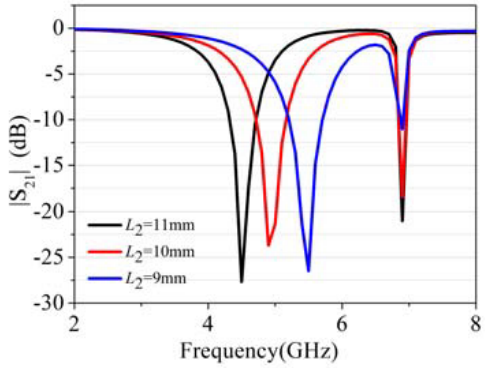

Figure 5. Variation of the frequency response of the S-parameter with L_2.

resonators are printed on the top side, and the ground plane is on the bottom side. It is fabricated on a substrate with relative dielectric permittivity of 2.65 and thickness of 1 mm. The parameters of the structure are: $L_1 = 13.3$ mm, $L_2 = 13$ mm, $W_1 = 19$ mm, $W_2 = 3.8$ mm, $D_1 = 0.1$ mm, $D_2 = 0.3$ mm.

Figure 4 plots the S-parameter curves of the fundamental structure. As can be observed, it has two transmission zeros at 3.9 and 6.8 GHz corresponding to the attenuation level of 32.4 and 22.6 dB. The return losses are 0.08 and 0.60 dB, respectively.

From above results, it is shown that the frequency responses of the proposed structure can be influenced by the dimensions of the dumbbell-shaped resonator and U-shaped slot. Parametric analyses of L_2 and L_4 are respectively implemented. Figure 5 plots the effect of L_2 on S-parameter. With the decrease of L_2, TZ_1 shifts to the higher frequency band while TZ_2 gets little influenced. When $L_2 = 9.0$ mm, the location of TZ_1 is 4.5 GHz. When $L_2 = 10$ mm, the location of TZ_1 is 4.9 GHz. However, when $L_2 = 11$ mm, the location of TZ_1 is 5.5 GHz.

Then, Figure 6 depicts the variation of the frequency response of the S-parameter with l_4. In this case, L_2 is equal to 13 mm. As shown in Figure 6, when l_4 increases from 0.8 mm to 1.2 mm, TZ_2 shifts to the lower frequency band, but the location of TZ_1 remains unchanged. From above results, it can be concluded that TZ_1 is controllable through the U-shaped defected ground structure, while TZ_2 is controllable through the dumbbell-shaped resonator. When $l_4 = 0.8$ mm, the location of TZ_2 is 7.1 GHz. And when $l_4 = 1.0$ mm, the location of TZ_2 is 7.0 GHz. However, when $l_4 = 1.2$ mm, the location of TZ_2 is 6.8 GHz.

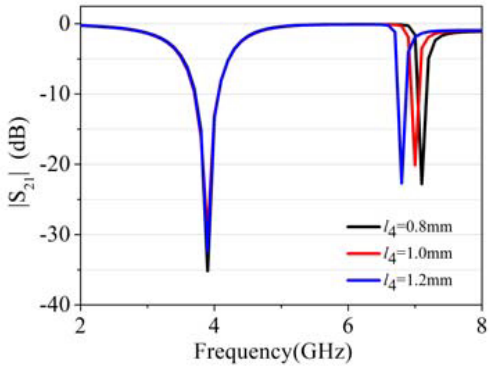

Figure 6. Variation of the frequency response of the S-parameter with l_4.

The proposed structure seems as two different transmission paths. The characteristics can be analyzed by adding their respective admittance matrixes which are transformed from the $ABCD$ parameter matrixes. They are $\begin{pmatrix} \cos\theta_1 & jZ_1\sin\theta_1 \\ \frac{j\sin\theta_1}{Z_1} & \cos\theta_1 \end{pmatrix}$ and $\begin{pmatrix} \cos\theta_2 & jZ_2\sin\theta_2 \\ \frac{j\sin\theta_2}{Z_2} & \cos\theta_2 \end{pmatrix}$, where θ_1 and θ_2 are the electrical lengths. The overall Y-matrix can be obtained through the proposed $ABCD$ matrixes. The overall Y-matrix is

$$\begin{pmatrix} \frac{\cos\theta_1}{jZ_1\sin\theta_1} + \frac{\cos\theta_2}{jZ_2\sin\theta_2} & \frac{-1}{jZ_1\sin\theta_1} - \frac{1}{jZ_2\sin\theta_2} \\ \frac{-1}{jZ_1\sin\theta_1} - \frac{1}{jZ_2\sin\theta_2} & \frac{\cos\theta_1}{jZ_1\sin\theta_1} + \frac{\cos\theta_2}{jZ_2\sin\theta_2} \end{pmatrix} \tag{3}$$

The transmission zeros are located at the frequencies where $|S_{21}| = 0$. So, the condition yields the relationship below. Solving it, the frequencies of transmission zero can be obtained.

$$\frac{\sin\theta_1}{\sin\theta_2} = \frac{-Z_2}{Z_1} \tag{4}$$

3. DESIGN OF DUAL-BAND BANDSTOP FILTER

Figure 7 depicts the top and bottom views of the design adopting four dumbbell-shaped resonators. The distances between dumbbell-shaped resonators are chosen as $L_3 = 1.9\,\text{mm}$ and $L_4 = 1.3\,\text{mm}$. These resonators have the same dimension. The size of the U-shaped defected ground structure is also fixed.

The transmission curves of the design adopting four dumbbell-shaped resonators are displayed in Figure 8(a). Compared with the result of fundamental structure adopting two resonators, the

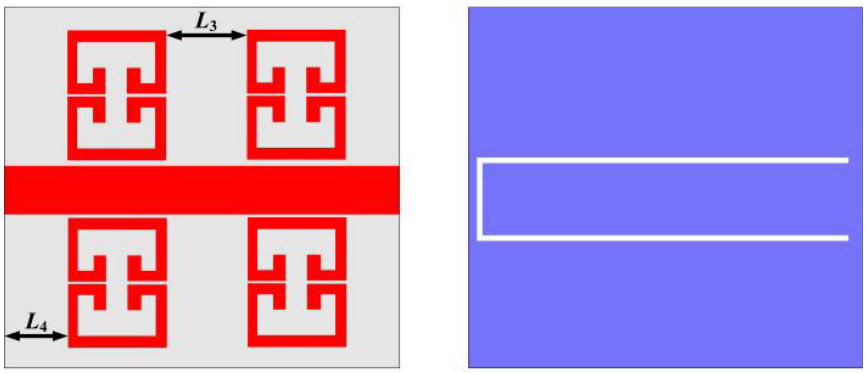

Figure 7. Configuration of structure adopting four dumbbell-shaped resonators. (a) Top view. (b) Bottom view.

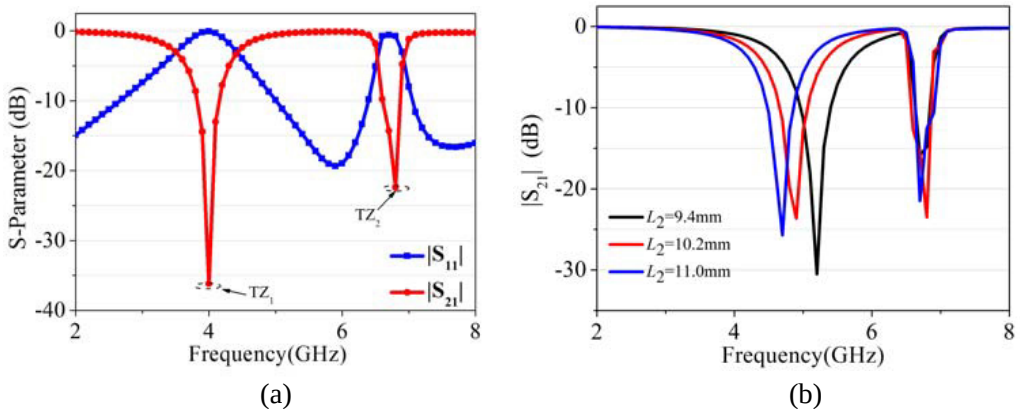

Figure 8. (a) The S-parameter curves of structure adopting four dumbbell-shaped resonators. (b) Variation of the frequency response of the S-parameter with L_2.

characteristics of selectivity and out of band suppression in each stopband are better. The return losses are 0.07 and 0.58 dB, respectively, and the characteristic of dual-band rejection is greater. So, it can be concluded that the characteristics of dual-band rejection get influenced by the number of dumbbell-shaped resonators. The variation of the frequency response of the S-parameter with L_2 is shown in Figure 8(b). When $L_2 = 9.4$ mm, the bandwidth of the first stopband is 440 MHz, and the location of transmission zero is 5.2 GHz. When $L_2 = 10.2$ mm, the bandwidth of the first stopband is 420 MHz, and the location of transmission zero is 4.9 GHz. However, when $L_2 = 11.0$ mm, the bandwidth of first stopband is 380 MHz, and the location of transmission zero is 4.7 GHz. Results show that the parameter of L_2 affects the location of the first stopband.

As shown in Figure 9, the structure of a dual-band bandstop filter is designed. It consists of eight dumbbell-shaped resonators and a transmission line. They are printed on the top side, while on the bottom side, it has two U-shaped slots. The detailed dimensions of the proposed filter are as follows: $L_5 = 0.9$ mm, $L_6 = 1.9$ mm, $L_7 = 2.2$ mm, $L_8 = 1.9$ mm, $D_3 = 0.3$ mm, and the total size of the fabricated structure is 37.3 mm × 19 mm. In addition, the S-parameter curves are demonstrated in Figure 10. It is observed that the characteristic of dual-band rejection are great. The center frequencies are respectively at 4 and 6.5 GHz with return losses of 0.04 and 0.20 dB, and the rejection levels of center frequencies are 41.9 and 26.1 dB. Detailed data show that the stopband return loss is less than 0.8 dB and is acceptable for the circuits fabricated on the substrate. Furthermore, on the right and left sides of each stopband, there are two transmission poles which induce sharp rejection response.

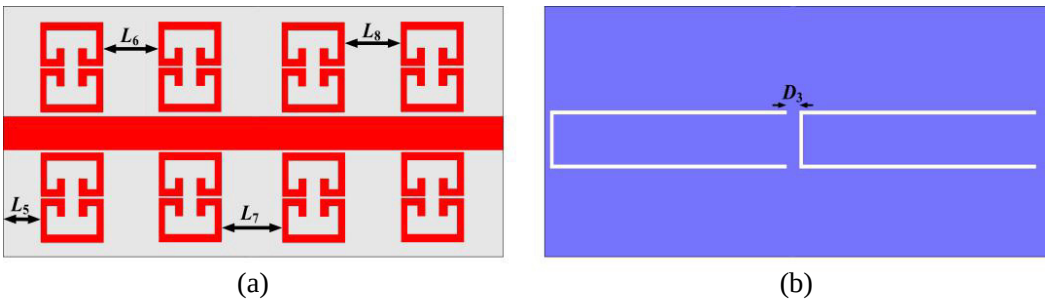

Figure 9. Configuration of proposed dual-band bandstop filter.

Based on the above-mentioned analysis, the first stopband depends on the U-shaped slot, and the second stopband is determined by the dumbbell-shaped resonator coupled to the main microstrip line. It is noted that these stopbands can be separately designed because they are induced through different current paths. As for the stopband design using the U-shaped slot and dumbbell-shaped resonator

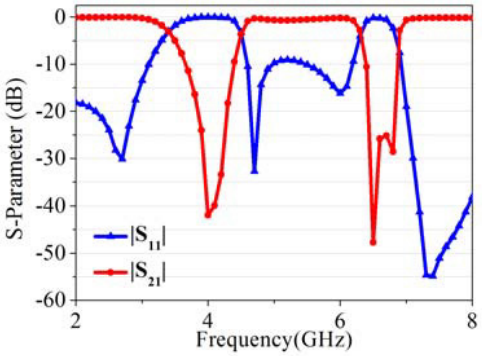

Figure 10. The S-parameter curves of proposed dual-band bandstop filter.

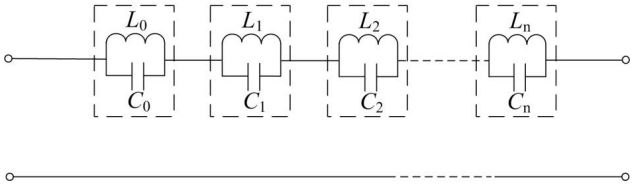

Figure 11. Equivalent circuit model for proposed bandstop filter.

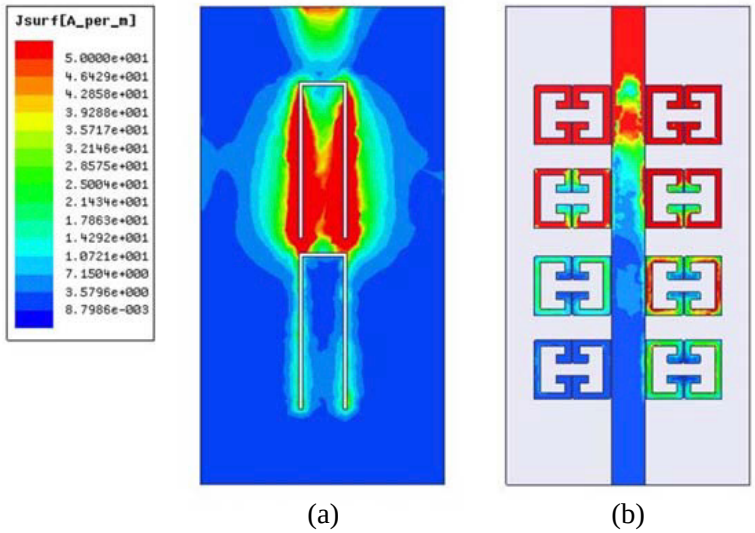

Figure 12. The surface current distributions at the frequencies of 4.0 and 6.5 GHz. (a) 4.0 GHz. (b) 6.5 GHz.

coupled to the main microstrip line, the equivalent circuit model for filter is plotted in Figure 11. The filter design with all relevant steps can be summarized as follows. The first step is circuit synthesis, which is based on the fractional bandwidth (FBW) and the operating frequency. The design parameters are obtained by

$$\Delta = (\omega_2 - \omega_1)/\omega_0 \tag{5}$$

$$Z_{0n} = \frac{4Z_0}{\pi g_n \Delta} \tag{6}$$

where Z_{0n} denotes the characteristic impedance of the resonator; Z_0 denotes the input and output impedance; g_n are the element values of lowpass prototype; ω_0 is the operating frequency; Δ is the fractional bandwidth. The second step is the design of dumbbell-shaped resonator coupled to the main microstrip line which induces stopband. According to the aforementioned formulas, the characteristic impedance of the resonator can be calculated. The third step is the design of a U-shaped slot which realizes another stopband. The fourth step is to use various dumbbell-shaped resonators with different coupling spaces to the main microstrip line. For simplicity, the sizes of dumbbell-shaped resonators are identical in order to make them have the same resonant frequency. The desired coupling space can be obtained by the full-wave EM solver.

As depicted in Figure 12, the surface current distributions at the frequencies of 4.0 and 6.5 GHz are given respectively. When the bandstop filter operates at 4.0 GHz, it can be observed that a large surface current density is induced on the U-shaped slot. When the filter operates at 6.5 GHz, a large surface current density is induced on the dumbbell-shaped resonators. So, it is demonstrated that when the filter operates at the stopbands, the energy is blocked in the process of transmission. It also proves the conclusions obtained in the parametric analysis of L_2 and L_4 in Section 2.

According to the results of the structure adopting two, four and eight dumbbell-shaped resonators, it can be found that as the number of resonators increases, the characteristic of dual-band rejection gets better. The characteristics of the structure adopting different numbers of dumbbell-shaped resonators are summarized in Table 2.

Table 2. Characteristics of structure adopting different numbers of dumbbell-shaped resonators.

Performance	Type A (two resonators)		Type B (four resonators)		Type C (eight resonators)	
In-band return loss (S_{11}) (dB)	0.08	0.60	0.07	0.58	0.04	0.20
In-band insertion loss (S_{21}) (dB)	32.4	22.6	36.1	22.4	41.9	26.1
Stopband bandwidth (MHz)	340	150	360	280	690	250

A photograph of the fabricated filter is shown in Figure 13(a). The frequency responses are measured through using the vector network analyzer. From the results depicted in Figure 13(b), the measured results agree with the simulation responses.

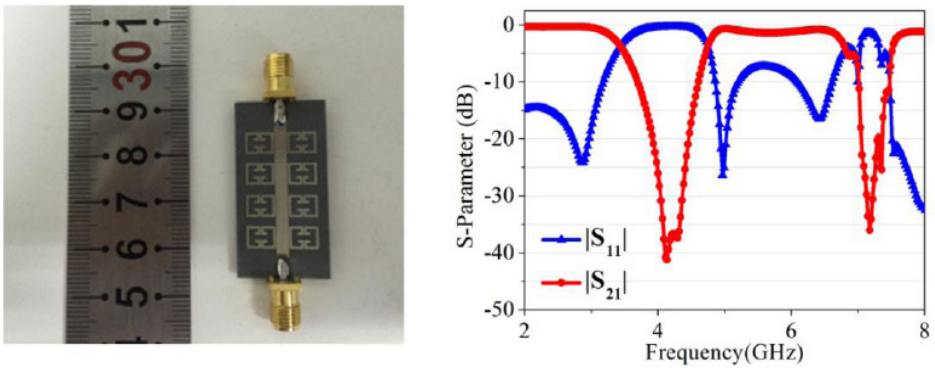

(a) (b)

Figure 13. (a) Photograph of the fabricated filter. (b) Measured frequency response of the dual-band bandstop filter.

4. CONCLUSION

In this letter, an implementation to design a dual-band bandstop filter adopting dumbbell-shaped resonators and U-shaped slots is presented. The integration of resonators and slot exhibits two transmission zeros which can be adjusted by tuning the parameters of the structure. Through adopting eight dumbbell-shaped resonators and optimizing the dimensions of structure, a dual-band bandstop filter with four transmission poles is fabricated. Measured results agree with the simulated ones. In addition, the structure is simple to design and quite compatible with planar construction fabrication.

REFERENCES

1. Pan, T., K. Song, and Y. Fan, "Compact dual-bandstop filter based on composite right/left handed transmission line," *Microwave and Optical Technology Letters*, Vol. 55, No. 5, May 2013.

2. Chin, K.-S., J.-H. Yeh, and S.-H. Chao, "Compact dual-band bandstop filters using stepped-impedance resonators," *IEEE Microwave and Wireless Components Letters*, Vol. 17, No. 12, December 2007.
3. Dhakal, R. and N.-Y. Kim, "A compact dual-band bandstop filter using a circular, folded, symmetric, meandered-line, stepped-impedance resonator," *Microwave and Optical Technology Letters*, Vol. 56, No. 10, October 2014.
4. Zhang, C., J.-P. Geng, R.-H. Jin, X.-L. Liang, and L. Liu, "Dual-wideband bandstop filter using stepped impedance coupled-lines," *Microwave and Optical Technology Letters*, Vol. 57, No. 10, October 2015.
5. Koirala, G. R., B. Shrestha, and N.-Y. Kim, "Compact dual-wideband bandstop filter using a stub-enclosedstepped-impedance resonator," *International Journal of Electronics and Communications (AEÜ)*, Vol. 70, 198–203, 2016.
6. Wang, W., M. Liao, Y. Wu, and Y. Liu, "Small-size high-selectivity bandstop filter with coupled-line stubs for dual-band applications," *Electron. Lett.*, Vol. 50, 286–288, 2014.
7. Chu, Q.-X. and L.-L. Qiu, "Sharp-rejection dual-band bandstop filter based on signal interaction with three paths," *Microwave and Optical Technology Letters*, Vol. 57, No. 3, 657–660, 2015.
8. Ning, H., J. Wang, Q. Xiong, and L.-F. Mao, "Design of planar dual and triple narrow-band bandstop filters with independently controlled stopbands and improved spurious response," *Progress In Electromagnetics Research*, Vol. 131, 259–274, 2012.
9. Dhakal, R. and N. Y. Kim, "A compact symmetric microstrip filter based on a rectangular meandered-line stepped impedance resonator with a triple-band bandstop response," *Sci. World J.*, Vol. 2013, 2013.
10. Jin, X. H., X. D. Huang, and C. H. Cheng, "Bandstop response of microstrip stepped impedance ring with rotational symmetry," *Electron. Lett.*, Vol. 49, 121–123, 2013.
11. Bakhit, A. A. and P. W. Wong, "A novel single and dual-band miniaturized matched band-stop filter using stepped impedance resonator," *Progress In Electromagnetics Research C*, Vol. 33, 229–241, 2012.
12. VeIidi, V. K. and S. Sanyal, "Compact planar dual-wideband bandstop filters with cross coupling and open-ended stepped impedance resonators," *ETRI Journal*, Vol. 32, No. 1, 2010.
13. Mashhadi, M. and N. Komjani, "Design of dual-band bandpass filter with improved upper stopband using novel stepped-impedance resonator," *Microwave and Optical Technology Letters*, Vol. 56, No. 3, 603–606, 2014.
14. Sarkar, P., M. Pal, and R. Ghatak, "A compact dual stopband bandstop filter using defected SIR and Hilbert shape fractal structure," *Microwave and Optical Technology Letters*, Vol. 58, No. 6, 1345–1347, 2016.
15. Che, W., W. Feng, and K. Deng, "Microstrip dual-band bandstop filter of defected ground structure and stepped impedance resonators," *International Journal of Electronics*, Vol. 97, No. 11, 1351–1359, 2010.
16. Pramod, K., K. Jugul, and A. K. Shrivastav, "Formulation of size reduction technique in microstrip circuits by using DGS and DMS," *Proceedings of the International Conference on Microwave*, 861–864, 2008.
17. Woo, D.-J., T.-K. Lee, J.-W. Lee, C. S. Pyo, and W. K. Choi, "Novel U-slot and V-slot DGSs for bandstop filter with improved Q factor," *IEEE Trans. Microwave Theory Tech.*, Vol. 54, 2840–2847, 2006.
18. Lee, S., S. Oh, W.-S. Yoon, and J. Lee, "A CPW bandstop filter using double hairpin-shaped defected ground structure with a high Q factor," *Microwave and Optical Technology Letters*, Vol. 58, No. 6, 1265–1268, 2016.
19. Woo, D.-J., T.-K. Lee, and J.-W. Lee, "An equivalent circuit model for a microstrip line with an asymmetric spiral-shaped defected ground structure," *Microwave and Optical Technology Letters*, Vol. 56, No. 5, 1222–1224, 2014.